SCIENTIFIC REPORTS

OPEN

Design of all-optical, hot-electron current-direction-switching device based on geometrical asymmetry

Chathurangi S. Kumarasinghe[1], Malin Premaratne[1], Sarath D. Gunapala[2] & Govind P. Agrawal[3]

We propose a nano-scale current-direction-switching device(CDSD) that operates based on the novel phenomenon of geometrical asymmetry between two hot-electron generating plasmonic nanostructures. The proposed device is easy to fabricate and economical to develop compared to most other existing designs. It also has the ability to function without external wiring in nano or molecular circuitry since it is powered and controlled optically. We consider a such CDSD made of two dissimilar nanorods separated by a thin but finite potential barrier and theoretically derive the frequency-dependent electron/current flow rate. Our analysis takes in to account the quantum dynamics of electrons inside the nanorods under a periodic optical perturbation that are confined by nanorod boundaries, modelled as finite cylindrical potential wells. The influence of design parameters, such as geometric difference between the two nanorods, their volumes and the barrier width on quality parameters such as frequency-sensitivity of the current flow direction, magnitude of the current flow, positive to negative current ratio, and the energy conversion efficiency is discussed by considering a device made of $Ag/TiO_2/Ag$. Theoretical insight and design guidelines presented here are useful for customizing our proposed CDSD for applications such as self-powered logic gates, power supplies, and sensors.

Highly enhanced electric fields produced by localized surface plasmons inside plasmonic nano-particles can generate a high-energy non-equilibrium electron gas[1,2] referred to as hot electrons. A fraction of these hot electrons often have sufficient momentum to cross the potential barrier at the nano-particle boundary and enter neighboring materials[3,4]. This is a fundamental process that has been found useful for many applications such as photovoltiacs[5,6], photocatalysis[3,7,8], nano-scale imaging[9] and photodetection[10]. In this paper we exploit this process for designing a novel optically controlled, current-direction-switching device.

The number and the energy distribution of hot electrons generated inside a nano-particle depends strongly on its shape and size[1,2], in addition to the nature of its composition, excitation power, excitation frequency, and dielectric properties of the surrounding medium[11,12]. Therefore, when two nano-particles that are dissimilar in shape or size are optically excited under similar conditions, one nano-particle can be expected to produce more higher energy electrons than the other due to this geometrical asymmetry. If they are separated by a finite potential barrier, a net flow of electrons (i.e., a net photo-current) from one particle to the other can be expected. Moreover, the direction and the magnitude of this current would depend on the excitation frequency. This process will leave one nano-particle positively charged and the other negatively charged. When an electron donor/receptor mechanism, such as an external circuit connecting both nano-particles, is available to transport the transferred holes/electrons and to maintain the charge neutrality, a continuous net electron flow can be expected. Clearly, this process can be exploited to develop a novel optically controllable nano-scale circuit element, capable of absorbing energy from an optical field to drive a current in the connected circuit, with the direction of the current switched via the applied field frequency. Moreover, the ability to control the internal electric field enhancement and the quantum-mechanical properties of nano-particles via their composition, shape and dimensions[2,13] gives one the flexibility for tailoring the switching frequencies of such devices. Owing to this behaviour, we refer to

[1]Advanced Computing and Simulation Laboratory (AλL), Department of Electrical and Computer Systems Engineering, Monash University, Clayton, Victoria 3800, Australia. [2]Jet Propulsion Laboratory, California Institute of Technology, Pasadena, CA 91109, USA. [3]The Institute of Optics, University of Rochester, Rochester, New York 14627, USA. Correspondence and requests for materials should be addressed to C.S.K. (email: chathurangi.kumarasinghe@monash.edu)

such a devices as the current-direction-switching-device (CDSD) in this paper. Such nanoscale, optically controlled, power supply devices will allow designing self-powered logic-gates for energy/information processing, bio-sensors, optical sensors and power supply units, leading to nano and molecular circuits that can function without external wiring.

Similar CDSDs based on semiconductor-semiconductor or semiconductor-metal structures[14–16] and molecules[17–20] have been reported in literature. However, in almost all cases they are based on fluid solutions and consist of subtle molecules or semiconductors, acting as light harvesting media. Their operation is mainly based on difference in material properted rather than difference in geometry, requiring multiple complex materials for construction. To our knowledge, the possibility of switching a plasmon-induced photo-current direction based on the geometrical asymmetry of nano-particles has not been discussed so far in the published literature. Such systems can offer higher mechanical and chemical stability than the existing fluid-based molecular systems. Furthermore, the use of metallic nano-particles as a light-harvesting medium is more desirable compared to bulk-metals, semiconductors or molecules, since plasmon-enhanced electric fields in metallic nano-particles can generate hot electrons more efficiently than the direct electron excitation mechanism used in other media. However, molecular-scale components have the potential for higher packing densities enabling highly miniaturized electronic circuits. Therefore, a hybrid approach involving a combination of molecular components with nano-scale power supply may be better suited in practice for developing electronic circuits.

It has been shown experimentally in the context of light-harvesting applications that a sustainable electron flow in a circuit based entirely on optically excited electrons generated from a metallic nano-structure is possible[3,4,21]. For example, an efficient solar water-splitting system with light as the only energy input has been demonstrated[3]. Its operation is based on Ag nanorods with TiO_2 caps that are submerged in water. A portion of electrons generated in an Ag nanorod passes through TiO_2 and is eventually transferred to ionized hydrogen in water, generating H_2 and leaving the nanorod positively charged. Electrons from the oxygen ions enter the Ag nanorod to resupply it with electrons, ultimately creating an electric circuit for the electron flow. Also, the ability to extract and inject hot electrons from plasmonic nano-particles to molecular electronic devices, has been experimentally demonstrated in a system consisting of Au nano-particles linked to thiophenylethynyl-terminated porphyrin molecules[6] where a hot-electron based current was clearly observed in the molecular structure. Such observations confirm the possibility of generating a continuous photo-current from plasmonic nano-particles that can be injected to a molecular- or nano-structure[22] acting as the external circuit.

The efficiency of hot-electron generation and injection depends significantly on the frequency-dependant enhancement of the electric field inside a nano-particle, which is essentially decided by its shape. Rod-like or ellipsoidal shapes supporting a longitudinal plasmon resonance have been proven to be more efficient than other basic shapes such as nanospheres, nanocubes or nanopallets[1,2]. Furthermore, the direction of the applied electric field relative to the nano-particle-barrier interface has a high influence on the generation of hot electrons with correct momentum orientation for injection over the barrier. Therefore, when designing self-powered hot-electron based CDSDs, a 'rod-like' shape is most suitable for the plasmonic nano-particle together with an optical field polarized along its longitudinal direction.

The non-equilibrium excited electrons relax into lower energy levels by emitting photons, distributing their energy to other electrons (in several hundred femtoseconds), and transferring energy to the lattice within a few picoseconds[23–25]. For this reason, the injection of hot-electrons over an energy barrier should happen before electrons lose energy through relaxation processes. On the other hand, such fast relaxation allows the hot-electron-based devices to have switching speeds approaching terahertz frequencies[26].

In this work, we have designed an all-optical, nano-scale, hot-electron CDSD by using two dissimilar metallic nanorods, separated by a thin potential barrier in the middle. The proposed structure require only two materials that can be found in abundance: a plasmonic metal such as gold or silver and a wide-band-gap semiconductor such as TiO_2. Such a device is easy to fabricate and is also economical compared to most other existing designs found in literature, which are made of complex molecules or multiple semiconductor-insulator layers. A continuous photo-current with the direction controllable via the operating frequency, can be injected from this CDSD to a molecular or a nano-structures acting as the external circuit. Moreover, since this CDSD is powered and controlled optically, it can be used to build all-optical nano/molecular circuits.

Typically, Fowler's theory is used to quantify the rate of electron injection from a metal to another material in contact[27]. This theory assumes an isotropic distribution of electron momentum orientations inside the metal, which is not the case for small nano-particles with dimensions less than the electron mean free path[28]. At energies close to the Fermi energy, the electron mean free path for metals used for hot electron generation such as silver and gold have reported values of 50 nm and 40 nm, respectively[29,30]. Therefore, for nano-structures such as the ones used in our design, a quantum-mechanical model incorporating the shape, size and composition specific effects of nonuniform electron energy distribution has to be developed. We model the behaviour of electrons inside the plasmonic nano-particles of our proposed CDSD by using the wave function for an electron confined to a finite potential well and consider the effect of the internal electric field as a periodic perturbation causing electronic transitions among energy levels. Similar models have been successfully applied for modeling hot-electron generation in isolated geometries such as nanorods, nano-pallets, nano-cubes[1,2,31], and nanospheres[32]. These results have been successfully matched with those obtained with the density functional theory (DFT), an high-accuracy ab-initio approach that includes quantum-mechanical many-body effects but is limited to smaller nano-particles (dimensions < 5 nm) owing to its excessively high computational costs.

Theoretical Formulation

As shown in Fig. 1, we consider two metallic nanorods of different lengths L_1 and L_2 but the same radius R. Both nanorods are made of the same material but are separated by a thin potential barrier of width w. The barrier height is given by $U_1 = \mathcal{E}_F + e\phi_B$, where $\mathcal{E}_F$ is the Fermi level of the metallic nanorods and $e\phi_B$ is the potential
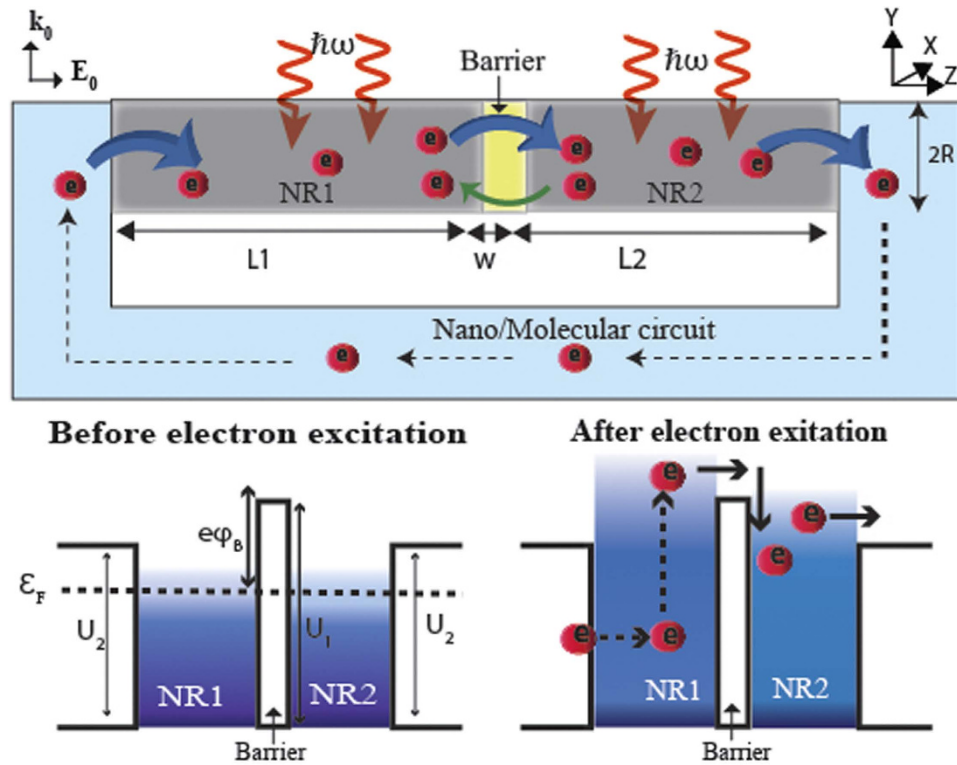
Figure 1. Schematic showing generation of hot electrons inside two metallic nanorods (NR1 and NR2) and their injection from one nanorod to the other over a potential barrier. The incident light is propagating in the direction of the wave vector $\mathbf{k_0}$ with its electric field $\mathbf{E_0}$ oriented along the length of nanorods. The bottom part shows the energy-band diagrams before and after the optical excitation.

difference between $\mathcal{E}_F$ and the conduction band of the barrier material (see the bottom part of Fig. 1). We assume that our structure is connected to an external circuit that allows flow of electrons. As seen in the figure, U_2 is the potential-barrier between the external circuit and the nano-particle.

When the nanostructure shown in Fig. 1 is optically exited with an electric field oriented along the nanorod length, hot electrons are generated in both nanorods. A fraction of these electrons attain sufficiently high energy with desired momentum orientation to cross the potential-barrier in the center and enter the neighboring nano-rod. The electric field enhancement in two nanorods is different owing to the difference in their lengths. Also, the electron wave-functions and energy levels in each are different due to differences in electron confinement. Consequently, the energy distribution of hot electrons generated and the number of electrons that cross the potential-barrier turn out to be unequal for each nanorod. This results in a net electron flow across the barrier from one nanorod to the other, generating a net electron flow in the connected external circuit. Since, which nanorod generates more high-energy electrons is decided by the excitation frequency, the direction of the net current flow over the barrier is controllable via the excitation frequency. In this paper, we refer to current flow from NR_1 to NR_2 as being positive (and from NR_2 to NR_1 as being negative).

In the following, we first outline the procedure for deriving a general expression for the net electron flow over the potential-barrier separating two nano-particles. Then we apply this expression to the nanostructure in Fig. 1 by calculating the wave functions and electron energy levels for the nanorods in the presence of an internal electric field while also paying attention to the specific nature of their boundaries.

General expression for the rate of electron flow. As discussed in the Methods section, the time-dependent transition probability for an electron from an initial state i to a final state f under an external perturbation $V'(\mathbf{r}, t)$ can be written as

$$P_{if}(t) = \left| -\frac{1}{j\hbar} \int_0^t \left\langle \psi_f(\mathbf{r}) | V'(\mathbf{r}, t') | \psi_i(\mathbf{r}) \right\rangle \exp(j\omega_{fi} t') \, dt' \right|^2,$$

(1)

were $\hbar = h/(2\pi)$, h is the Plank's constant, t is the time measured from the start of the perturbation, $\psi_f(\mathbf{r})$ and $\psi_i(\mathbf{r})$ represent electron's wave functions in the final and the initial states, and ω_{fi} is the energy difference between these two states. The rate of electron excitation $\mathbb{R}_{if}(\omega)$ can be obtained by taking the derivative of $P_{if}(t)$ with respect to time. For a sinusoidal perturbation at frequency ω, i.e. $V'(\mathbf{r}, t) = V'(\mathbf{r})[\exp(j\omega t) + \exp(-j\omega t)]$, this rate is found to be

$$\mathbb{R}_{if}(\omega) = 2\pi\hbar \, |\langle\psi_f(\mathbf{r})|V'(\mathbf{r})|\psi_i(\mathbf{r})\rangle|^2 \delta_{\mathcal{E}_f - \mathcal{E}_i, \hbar\omega}, \tag{2}$$

where $\mathcal{E}_i$ and $\mathcal{E}_f$ are eigen-energies of the initial and the final states of the transition and $\delta_{\mathcal{E}_f - \mathcal{E}_i, \hbar\omega}$ is the Dirac delta function.

In deriving Eq. (2) from Eq. (1) we have assumed that the duration of the perturbation, t is much greater than the electron relaxation time associated with electron-electron collisions[33,34]. This allows us to use the approximation

$$\lim_{t\to\infty} \frac{\sin^2((\omega_{fi} - \omega)t/2)}{(\omega_{fi} - \omega)^2 t^2/4} = \frac{2\pi\hbar}{t} \delta_{\mathcal{E}_f - \mathcal{E}_i, \hbar\omega}. \tag{3}$$

Electrons that are excited to high energy states either surmount the potential barrier and reach the other nano-particle or reflect off the barrier due to scattering events. The probability of an electron with energy $\mathcal{E}_f$ crossing the barrier can be written as[35,36],

$$P_{\text{barrier}}(\mathcal{E}_f) = \exp\left(-\frac{w}{\tau_s}\sqrt{\frac{m'}{2\mathcal{E}_f}}\right), \tag{4}$$

where m' is electron's effective mass and τ_s is electron's scattering time in the barrier. As expected, higher energy electrons have a larger probability of crossing the barrier. In nanometer-sized semiconductor particles, the magnitude of band bending is negligibly small[37,38] and therefore safely discarded in our derivations.

By summing $\mathbb{R}_{if}(\omega)$ over all possible initial and final electron states and accounting for the barrier loss and electron availability, the transfer rate of hot electrons from one nano-particle to the other nano-particle can be obtained as

$$\mathbb{N}(\omega) = \sum_i \sum_f \mathbb{R}_{if}(\omega) P_{\text{barrier}}(\mathcal{E}_f) f_F(\mathcal{E}_i)(1 - f_F(\mathcal{E}_f)), \tag{5}$$

with $f_F(\mathcal{E}_k)$ indicating the Fermi distribution associated with an electron of energy $\mathcal{E}_k$. The multiplication factors $f_F(\mathcal{E}_i)$ and $(1 - f_F(\mathcal{E}_f))$ account for the the probability of finding an electron in the initial state i and the probability of finding the final state f empty during a transition. This equation has been multiplied by a factor of 2 to account for electron's spin and by a factor of 1/2 to account for the probability of the excited electron having its momentum towards the barrier (instead of the opposite direction). However, the two factors simply cancel each other.

If $\mathbb{N}(\omega)_{\text{particle1}}$ and $\mathbb{N}(\omega)_{\text{particle2}}$ represent the hot-electron transfer rates from each nano-particle to the other particle, the general expression for the electron flow rate between the CDSD and the external circuit can be written as

$$\mathbb{I}(\omega) = \mathbb{N}(\omega)_{\text{particle1}} - \mathbb{N}(\omega)_{\text{particle2}}. \tag{6}$$

This equation can be used for any nano-particle shape after substituting relevant perturbing potentials along with electron wave functions and energy levels. In the following sections we apply it for the CDSD described in Fig. 1 and consisting of two nanorods.

Perturbing potential inside the nanorods. The time-dependent external electric field $\mathbf{E}_0(\omega)[\exp(j\omega t) + \exp(-j\omega t)]$ of the incident light is assumed to be linearly polarized along the longitudinal axis of nanorods since longitudinal modes of electrons show higher field enhancement than the transverse modes in rod-like shapes[39]. We write the amplitude of the internal electric field in the form $\mathbf{E}(\omega) = \gamma(\omega)\mathbf{E}_0(\omega)$, where $\gamma(\omega)$ is the the enhancement factor induced by localized surface plasmons. This factor depends strongly on the shape of the nano-particle and its orientation with respect to the applied field, in addition to the dielectric properties of the nano-particle and the surrounding medium[40]. Since it is known that the plasmonic behaviour of a rod-like shape is quite close an ellipsoid when its aspect ratio (length/radius) is high, we assume that the internal electric field is oriented parallel to the external field[41,42]. The enhancement factor then takes the form[1],

$$\gamma(\omega) = \sqrt{\frac{1}{\wp}\int_\wp \frac{|\mathbf{E}(\omega)|^2}{\mathbf{E}_0(\omega)^2}dV}, \tag{7}$$

where $\wp$ is the volume of the nano-particle.

The perturbing potential can now be written considering $\mathbf{r} = (\rho, \Phi, z)$ in cylindrical coordinated as

$$V'(\mathbf{r}) = q\gamma(\omega)\mathbf{E}_0(\omega)z, \tag{8}$$

where q is the charge of an electron. By substituting Eq. (8) in Eq. (2) we obtain the electron transition rate as

$$\mathbb{R}_{if}(\omega) = \frac{2\pi\hbar^3(q\gamma(\omega)E_0)^2}{\mu^2(\mathcal{E}_f - \mathcal{E}_i)^2} \left| \left\langle \psi_f(\mathbf{r}) \left| \frac{\partial}{\partial z} \psi_i(\mathbf{r}) \right\rangle \right|^2 \delta_{\mathcal{E}_f - \mathcal{E}_i, \hbar\omega}.$$

(9)

Here, we have used the quantum mechanical relationship between the position operator $\mathbf{r}$ and the momentum operator $\hat{p} = -j\hbar\nabla$ in the form[43],

$$\langle\Psi_f(\mathbf{r})|\mathbf{r}|\Psi_i(\mathbf{r})\rangle = \frac{j\hbar}{\mu(\mathcal{E}_f - \mathcal{E}_i)} \langle\Psi_f(\mathbf{r})|\hat{p}|\Psi_i(\mathbf{r})\rangle.$$

(10)

Energy eigenstates of an electron inside a nanorod. Assuming that conduction electrons in a metallic nanorod act as free particles in a cylindrical potential well and the nanorod boundary acts as an infinite potential-barrier except in the longitudinal direction, the Schrödinger equation for a single electron can be written in cylindrical coordinates as

$$\left(-\frac{\hbar^2}{2\mu}\nabla^2 + V(\rho, \Phi, z)\right)\psi_k(\rho, \Phi, z) = \mathcal{E}_k\psi_k(\rho, \Phi, z),$$

(11)

with the confining potential $V(\rho, \Phi, z)$ given by

$$V(\rho, \Phi, z) = \begin{cases} 0 & \text{if } \rho \le R \text{ and } L \ge z \ge 0 \\ U_1 & \text{if } \rho \le R \text{ and } z < 0 \\ U_2 & \text{if } \rho \le R \text{ and } z > L \\ \infty & \text{otherwise} \end{cases},$$

(12)

where L is the length of the nanorod under consideration. As shown in Fig. 1, U_1 and U_2 denote the heights of the potential barriers on two sides of a nanorod. Owing to the cylindrical symmetry, we can employ the method of separation of variables and write the wave function in the form

$$\psi_k(\mathbf{r}) = \psi_{n,m}(\rho)\psi_m(\Phi)\psi_l(z),$$

(13)

where the integers $n \ge 0, |m| \ge 0$ and $l \ge 0$ are quantum numbers corresponding to a particular electron state k. Here, $\psi_{n,m}(\rho), \psi_m(\Phi)$, and $\psi_l(z)$ represent the radial, azimuthal and longitudinal components of the wave function respectively. The electron energy of state k can be written as,

$$\mathcal{E}_k = \mathcal{E}_{n,m} + \mathcal{E}_l,$$

(14)

with $\mathcal{E}_{n,m}$ representing the radial and azimuthal components and $\mathcal{E}_l$ representing the longitudinal component.

After applying the orthonormal property of the radial and azimuthal components of the wave function we can simplify Eq. (9) as

$$\mathbb{R}_{if}(\omega) = \frac{2\pi\hbar^3(q\gamma(\omega)E_0)^2}{\mu^2(\mathcal{E}_f - \mathcal{E}_i)^2} \left| \int_0^L \psi_{lf}(z)\frac{\partial}{\partial z}\psi_{li}(z)\,dz \right|^2 \delta_{nf,ni}\delta_{mf,mi}\delta_{\mathcal{E}_f - \mathcal{E}_i, \hbar\omega},$$

(15)

where the quantum numbers mi, ni and li coorespond to state i and mf, nf and lf correspond to state f. It is clear in Eq. (15) that the conditions $mi = mf$ and $ni = nf$ are required for $\mathbb{R}_{if}(\omega)$ to be non-zero, and we need to consider in our analysis only those transitions that change the longitudinal quantum number. Physically, this condition is imposed because the applied electric field is along the longitudinal axis of the nanorod, and the internal electric field is in the same direction as the applied field.

The electron is confined by infinite boundaries in radial and azimuthal directions according to Eq. (12) and therefore the quantized electron energies $\mathcal{E}_{mi,ni}$ and $\mathcal{E}_{mf,nf}$, required for further calculations can be easily found as shown in the Methods section. However, finding the longitudinal components $\psi_{li}(z), \psi_{lf}(z), \mathcal{E}_{li}$ and $\mathcal{E}_{lf}$ is more complicated owing to the finite nature of longitudinal boundaries. To find these we assume that prior to excitation electrons reside in an energy state below the Fermi level $\mathcal{E}_F$, which is less than both U_1 and U_2, and all final energy states of interest have longitudinal energies larger than U_1 and U_2. As shown in the Methods sections, two sets of solutions needs to be found for Eq. (11) for these two situations[33]. From these solutions it is clear that $\mathcal{E}_i$ is quantised. However, $\mathcal{E}_f$ is not quantized because $\mathcal{E}_{lf}$ is continuous as it is greater than both U_1 and U_2 i.e., in the final state the electron is unconfined in the longitudinal direction.

Electron flow over the barrier as a function of frequency. After substituting the initial and final wave functions derived in the Methods section (Eqs (30) and (36)) into Eq. (15), we obtain the transition rate in the form

$$\mathbb{R}_{if}(\omega) = \frac{2\pi\hbar^3(q\gamma(\omega)E_0)^2}{\mu^2(\mathcal{E}_f - \mathcal{E}_i)^2} \left| \frac{\Omega(L, \mathcal{E}_i, \mathcal{E}_f)}{\sqrt{L_{\inf}}} \right|^2 \delta_{nf,ni}\delta_{mf,mi}\delta_{\mathcal{E}_f - \mathcal{E}_i, \hbar\omega},$$

(16)

where,

$$\Omega(L, \mathcal{E}_i, \mathcal{E}_f) = k_{2li}\left[\frac{\overline{C_{lf}}C_{li}(\exp(j(k_{2li} + k_{2lf})L) - 1)}{(k_{2li} + k_{2lf})}\right.$$
$$- \frac{C_{li}\overline{D_{lf}}(\exp(-j(k_{2lf} - k_{2li})L) - 1)}{(k_{2lf}x - k_{2li})}$$
$$- \frac{D_{li}\overline{C_{lf}}(\exp(j(k_{2lf} - k_{2li})L) - 1)}{(k_{2lf} - k_{2li})}$$
$$\left. + \frac{D_{li}\overline{D_{lf}}(\exp(-j(k_{2lf} + k_{2li})L) - 1)}{(k_{2lf} + k_{2li})}\right]. \tag{17}$$

In the Methods section it is described how to find the values of C_{li}, $\overline{C_{lf}}$, D_{li}, $\overline{D_{lf}}$, k_{2li} and k_{2lf} in terms of L, $\mathcal{E}_i$ and $\mathcal{E}_f$. The variable L_{inf} is a fictitious length of confinement that is introduced for the ease of final eigen states derivation, which is removed at a later stage.

Because of the existence of a continuum of final states we can write the summation over discrete final states in Eq. (5) as an integration over energy $\mathcal{E}_f$[43]. The result is

$$\mathbb{N}(\omega) = \sum_i \int \mathbb{R}_{if}(\omega)P_{\text{barrier}}(\mathcal{E}_f)(\omega)f_F(\mathcal{E}_i)(1 - f_F(\mathcal{E}_f))\frac{L_{\text{inf}}}{\pi\hbar}\sqrt{\frac{m}{2\mathcal{E}_f}}d\mathcal{E}_f. \tag{18}$$

We can safely approximate the probabilities of finding the state $\mathcal{E}_i$ occupied and state $\mathcal{E}_f$ empty given by $f_F(\mathcal{E}_i)$ and $\left(1 - f_F(\mathcal{E}_f)\right)$ as unity because $\mathcal{E}_i < \mathcal{E}_F$ and $\mathcal{E}_f > \mathcal{E}_F$ in all situations of interest. By substituting Eq. (16) in this equation, we finally obtain the bound-to-continuum electron transfer rate for a nanorod:

$$\mathbb{N}(\omega) = \frac{\sqrt{2}(q\gamma(\omega)E_0)^2}{\mu^{3/2}\omega^2}\sum_i\frac{|\Omega(L, \mathcal{E}_i, \mathcal{E}_i + \hbar\omega)|^2}{\sqrt{(\mathcal{E}_i + \hbar\omega)}}\exp\left(-\frac{w}{\tau_s}\sqrt{\frac{m}{2(\mathcal{E}_i + \hbar\omega)}}\right). \tag{19}$$

The electrons will initially occupy a state below the Fermi level. After the transition, in order to be injected to the barrier, electrons should have longitudinal energy greater than the barrier indicated by $\mathcal{E}_{lf} > U_1$. Therefore considering a linear single-photon absorption, the limits of the summation for the quantum number $i = \{mi, ni, li\}$ can be given as,

$$U_1 - \hbar\omega < \mathcal{E}_{li} \leq \mathcal{E}_F, \ \ 0 \leq \mathcal{E}_{ni,mi} \leq \mathcal{E}_F - \mathcal{E}_{li}. \tag{20}$$

The most important feature of Eq. (19) is that the electron transfer rate depends on the length of the nanorod and is different for the two nanorods in Fig. 1 because of their different lengths. We can calculate the net current flowing through the circuit by using

$$\mathbb{I}(\omega) = \mathbb{N}(\omega)_{NR_1} - \mathbb{N}(\omega)_{NR_2} \tag{21}$$

where the subscripts indicate the two nanorods of different lengths. We present the numerical results based on Eqs (19) and (21) in the next section.

Results and Discussion

We consider a CDSD whose two nanorods made of silver are separated by a thin TiO$_2$ barrier. TiO$_2$ is selected as the barrier material because it has a wide-band-gap of 3.3 eV and it does not absorb radiation below this band-gap value. Therefore, in the frequency range 1.5 to 3.3 eV, we can neglect any contribution from excited electrons in TiO$_2$ to the net electron flow. It is important that the barrier material does not generate excited electrons contributing to the electron flow because we do not have control over the direction of such electrons. Also it could create more resistance for the electrons crossing the barrier. Silver is selected as the plasmonic metal for the nanorods due to its strong interaction with light.

The parameter U_1 can be found as $\mathcal{E}_F + e(\phi_m - \chi)$, where ϕ_m is the work function of Ag (in the range 4.26–4.72 eV)[44] and χ is the electron affinity of TiO$_2$ films (about 3.9 eV)[45–47]. This gives $U_1 = 0.8$ eV for our CDSD, and this barrier height is adjustable by changing the materials used. For example by using Ag with SiC poly-types for which the electron affinity can be varied between 2.33–4.00 eV[48,49], barrier height can be adjusted between 0.70–1.57 eV. For all calculations, we assume the potential-barrier U_2 between the nanorods and the external circuit is 0.5 eV.

Figure 2 shows the electric field distributions, electric field enhancement factors and the resulting hot-electron injection rates for the two nanorods along with their differences. It can be seen from Fig. 2(a) that electric field enhancement factors are different in the two nanorods, and this difference is frequency dependent, showing negative and positive peaks at certain frequencies. For instance, NR$_1$ is at resonance around 1.5 eV while NR$_2$ is not. Therefore, as shown in the cross section view, the electric field intensity inside NR$_1$ in general is much stronger than in NR$_2$ at this frequency, generating a field asymmetry inside the CDSD. This contributes to unequal hot electron generation in nanorods and as a result a net current flow from NR$_1$ to NR$_2$. However the field asymmetry
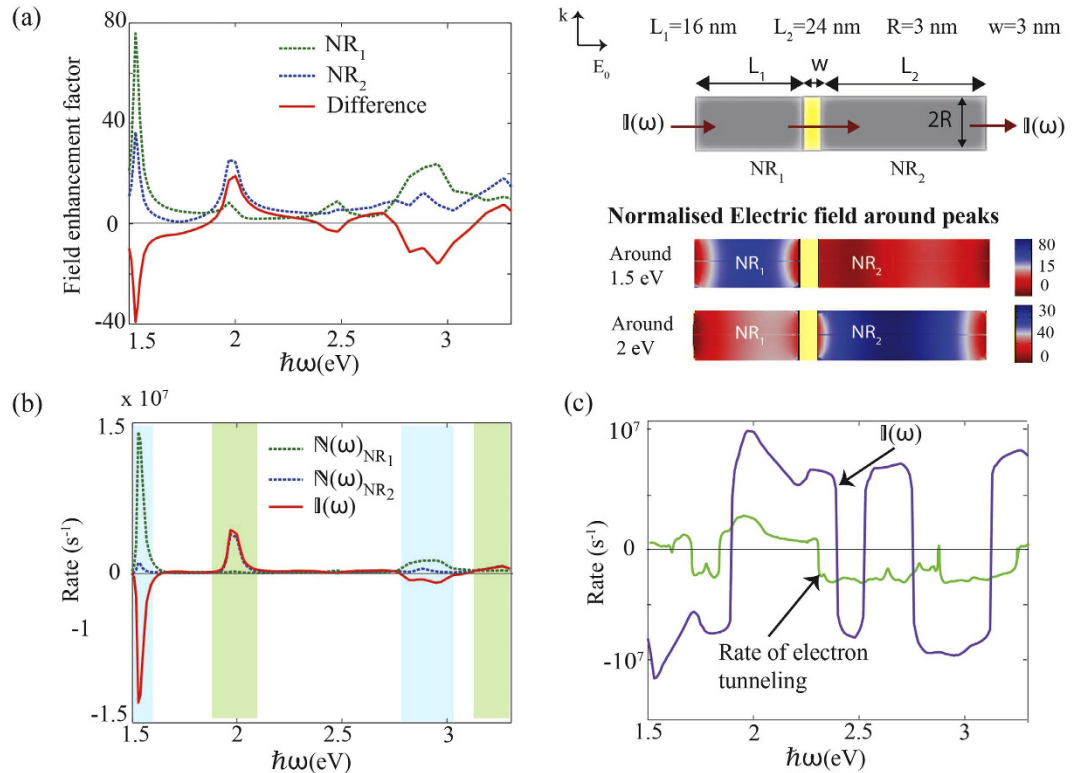
Figure 2. Hot-electron switching behaviour in two nanorods. (**a**) Electric-field enhancement factors ($\gamma(\omega)$) inside NR_1 and NR_2 and their difference. The Ag/TiO$_2$/Ag composite structure and its design parameters along with the normalised electric field ($\mathbf{E}(\omega)/\mathbf{E}_0(\omega)$) in a cross section of the device around the peaks 1.5 eV and 2 eV are shown on right. (**b**) Injection rates of hot electrons from NR_1 and NR_2 and the net current flow through the CDSD. The blue and green bands indicate the direction of current flow that can be switched by changing photon energy. (**c**) Comparison of net current through the CDSD and the tunnelling current through the barrier (on a log scale).

is reversed around 2 eV, where the electric field inside NR_2 in general appears to be much stronger than in NR_2 due to resonance, contributing to a net electron flow from NR_1 to NR_2. Figure 2(b) illustrates how the current flow over the barrier from each nanorod is variable with the frequency. When $\mathbb{I}(\omega)$ is positive, the current flow is from NR_1 to NR_2; the direction reverses when $\mathbb{I}(\omega)$ is negative. When comparing Fig. 2(a,b), it is apparent that, as a general trend, peak values in $\mathbb{I}(\omega)$ correspond to the peaks in the enhancement factor difference. Figure 2(c) shows $\mathbb{I}(\omega)$ on a logarithmic scale and shows more clearly the nature of frequency dependant direction switching. The main thing to note is that both the magnitude and the direction of net electron flow can be easily controlled by varying the excitation frequency.

Electrons with longitudinal energy less then the barrier height can still pass through the barrier via tunnelling. The tunnelling transmission coefficient for the barrier can be calculated using[33],

$$T(\mathcal{E}) = \left(1 + \frac{U_1{}^2}{4\mathcal{E}(U_1 - \mathcal{E})} \sinh^2\left(w\sqrt{\frac{2m(U_1 - E)}{\hbar^2}}\right)\right)^{-1}. \tag{22}$$

The tunneling-aided electron transmission rate can be calculated by summing up all energy states below U_1 multiplied by $T(\mathcal{E})$. However, it can be seen from Fig. 2(c) that for the electric field intensity (3.6×10^7 Wm^{-2}) and the barrier width of 3 nm that we have considered here, tunnelling current is negligible compared to $\mathbb{I}(\omega)$. Experimental studies also suggest that tunneling of electrons between plasmonic nano-particles is negligible for junction widths larger than 0.5 nm[50] under moderate electric field intensities used here.

In Fig. 3, we vary the length of one nanorod while keeping length of the other nanorod constant to study the effects of geometrical asymmetry on $\mathbb{I}(\omega)$. We introduce the parameter, $\zeta = (L_1 - L_2)/(L_1 + L_2)$, representing the relative length difference of two nanorods. It can be seen from Fig. 3(a) that as the value of L_2 gets closer to L_1 so that the absolute value of ζ becomes small, the oscillatory nature of $\mathbb{I}(\omega)$ becomes more pronounced, making the direction of the flow highly sensitive to the frequency. We define another parameter β to represents the ratio between average values of the current in the positive and negative directions. In designing CDSDs this ratio is an important parameter and its ideal value is close to unity. It can be seen from Fig. 3(b) as the absolute value of ζ
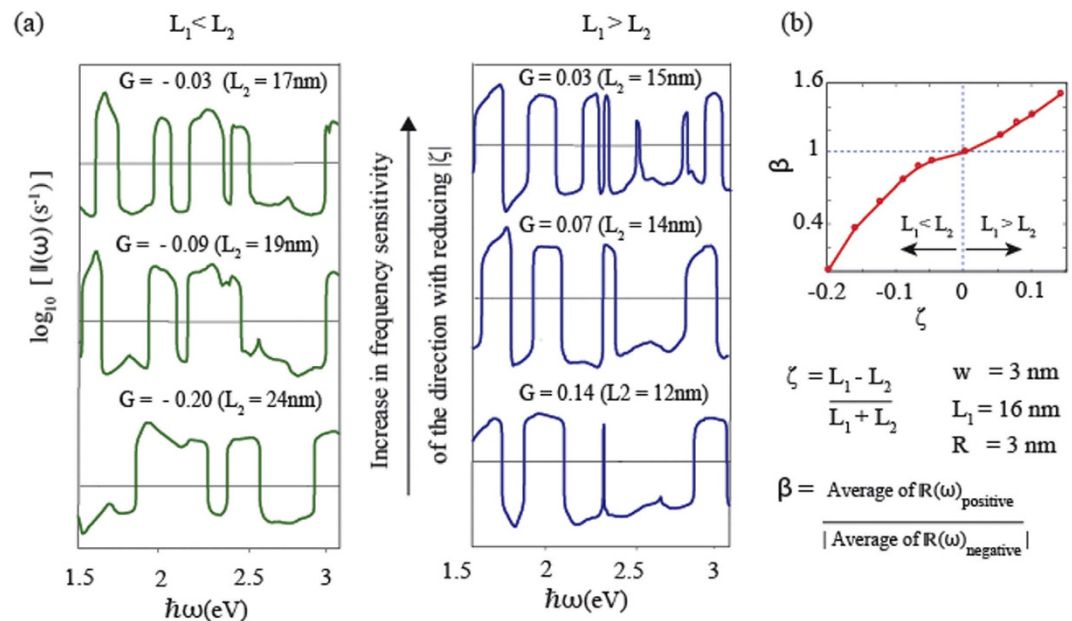
Figure 3. Effect of relative length difference. All parameters are the same as in Fig. 2 except L_2 is varied from 12 nm to 22 nm keeping L_1 and all other parameters constant. (**a**) $\mathbb{I}(\omega)$ as a function of photon energy on a log scale. (**b**) β as a function of ζ.

becomes large, β moves away from unity, indicating an increased difference between magnitudes of positive and negative currents.

Figure 4 shows the influence of relative nanorod length difference (ζ) and overall device volume on the energy conversion efficiency and the magnitudes of positive and negative current flows. The internal quantum efficiency (IQE) is a measure of energy conversion efficiency of a system and can be used as a figure of merit for comparison among different energy converting systems. For this nano-structure, IQE can be defined as the ratio of absorbed photons to injected net electrons over the barrier (see Methods). Figure 4(a) shows IQE for devices having different combination of L_1 and L_2 (i.e. different ζ values), while keeping total length $L_1 + L_2$ constant. It can be seen that the IQE exhibits an oscillatory behavior. However, note that the peak quantum efficiency can exceed 30% for $\zeta = 0.2$ at a certain excitation frequency. Figure 4(b) shows the averaged IQE over the total range of photon energies (1.5–3.2 eV) for different device volumes and ζ values. An increase in the value of ζ can increase the averaged IQE, indicating that a higher geometric difference can lead to higher efficiency. Further, for a certain ζ value, increasing the overall device volume can result in reduced averaged IQE. At the same time, since the number of conduction electrons increases with increasing volume, the magnitude of current flow (averaged over the spectrum), both positive and negative, increases with the volume as seen in Fig. 4(c). However, the the ratio between average positive to negative electron flow (β) remains almost constant despite of the change in volume, indicating it is mainly dependant on the geometrical deference indicated by ζ.

In Fig. 5, the barrier width is varied while keeping all the other factors constant. When the separation between nanorods is high, as seen in In Fig. 5(b), the difference between their electric field enhancements will also increase due to reduced electric field coupling between nanorods, which can contribute positively for improving $\mathbb{I}(\omega)$. On the other hand, the electron energy loss while crossing the barrier will increase with increasing w, which can have a negative effect on $\mathbb{I}(\omega)$. However, as seen in Fig. 5(a,c), the overall effect is a reduction in the net electron flow and the averaged IQE.

In our derivations, the duration of the electron excitation under the optical field is considered to be much greater the electron relaxation time associated with electron-electron collisions. Under such conditions, electrons achieve local equilibrium within the duration of the laser pulse and the metal nanoparticle thermodynamic state can thus be described by one temperature. Therefore the current injection rate from the CDSD to the external circuit is found to be independent of time during the process. For Ag, this electron relaxation time in literature is typically around 350 fs[24,51,52].

If the pulse duration is shorter than this electron relaxation time, the electron flow rate between the CDSD and the external circuit during and after the optical perturbation need to be studied in a high resolution femtosecond or picoseconds time scale emphasising non-equilibrium effects which is outside the scopes of this research. Under a picosecond pulse, before the end of the pulse, the electron gas achieves internal thermalization vial electron-electron collisions, whilst the electron-lattice system is still far from equilibrium. Under these conditions the classical two-temperature model[24,51,53] is used to model the time evolution of electron excitation rate due to energy exchange with the lattice. This energy exchange rate is proportional to the lattice-electron temperature difference and the electron-phonon coupling constant of the nanoparticle[24,53,54]. Under a femtosecond laser pulse, electron-electron collisions are not fast enough to thermalize the electron gas during the laser pulse, therefore the non-equilibrium conditions are maintained up to some hundreds of femtoseconds. Under this condition,
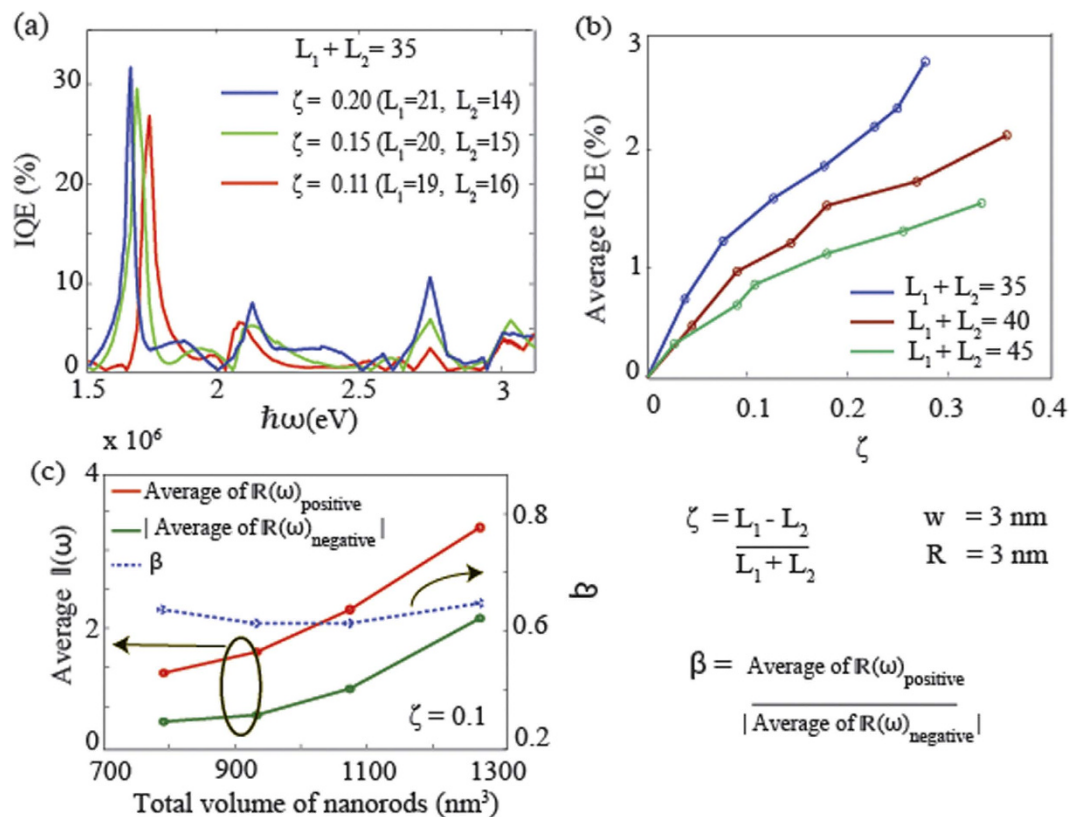
Figure 4. Same as in Fig. 2 except L_1 and L_2 are varied keeping the value $L_1 + L_2$ and other parameters constant. (**a**) $\mathbb{I}(\omega)$ in log scale for different L_1 and L_2 combinations. (**b**) Quantum efficiency for each case as a function of frequency. (**c**) Averaged quantum efficiency for each case against the ratio L_1/L_2.

the Boltzmann equation should be solved for both electrons and phonons, considering the Fermi-Dirac and Bose-Einstein statistics, respectively to calculate the energy distributions for the two systems.

A challenge in fabrication of any nano structure is to control the particle sizes, shapes and morphologies. Irregular shapes and sizes due to fabrication imperfections may change the electric field enhancement and the electron energy structure of the CDSD from expected values. The geometry of the tips of the rods have a significant impact on field enhancement, especially in smaller rods where the tips comprise a larger portion of the overall rod[55]. Sharper tips generate higher field enhancement and the lightning-rod effect can be seen in extreme cases[56].

Irregular surfaces with pits and bumps can be approximated roughly as an array small spherical or spheroidal particles, each having its own resonance frequency sitting on a flat surface[57]. If there are only few such irregularities, random peaks can be observed in the field enhancement spectra. If the surface is highly irregular containing pits and bumps of different sizes and shapes, it can broaden the peaks of the field enhancement spectrum due to combined effects, resulting in reduced frequency sensitivity for current direction switching.

The magnitude of the output is highly sensitive to the barrier width as discussed in the previous section. A few nanometre difference in the barrier thickness can cause a few orders of magnitude change in the output current. The current switching frequencies and internal quantum efficiencies can be considered as moderately sensitive to device dimensions.

Design Guidelines and Conclusion

We have proposed a composite nanostructure that is capable of generating a current flow in a connected circuit when light is incident on it. Moreover, both the direction and the magnitude of current is controllable via the frequency of the incident light. The device operation is based on the concept of hot-electron injection from two geometrically dissimilar nano-particles over a common barrier. We have derived the rate of electron flow in such a structure, made of two nanorods, by using the single-electron wave function and the corresponding eigen energy states of an electron inside each nanorod under a periodic perturbation. The electric field enhancement inside the structure, which has a high influence on the hot-electron generation rate was derived numerically.

We used our theoretical model to study how the current flow in our proposed CDSD depends on various design parameters. Our results show that the magnitude and the direction of current $\mathbb{I}(\omega)$ is highly controllable via the excitation frequency. Increase in the device volume can result in a decrease in the efficiency of the device and its suitability for nano/molecular scale designs. Further, if the nanorods have dimensions longer than the electron mean free path of the metal, electrons may relax before reaching the boundary, reducing the efficiency.
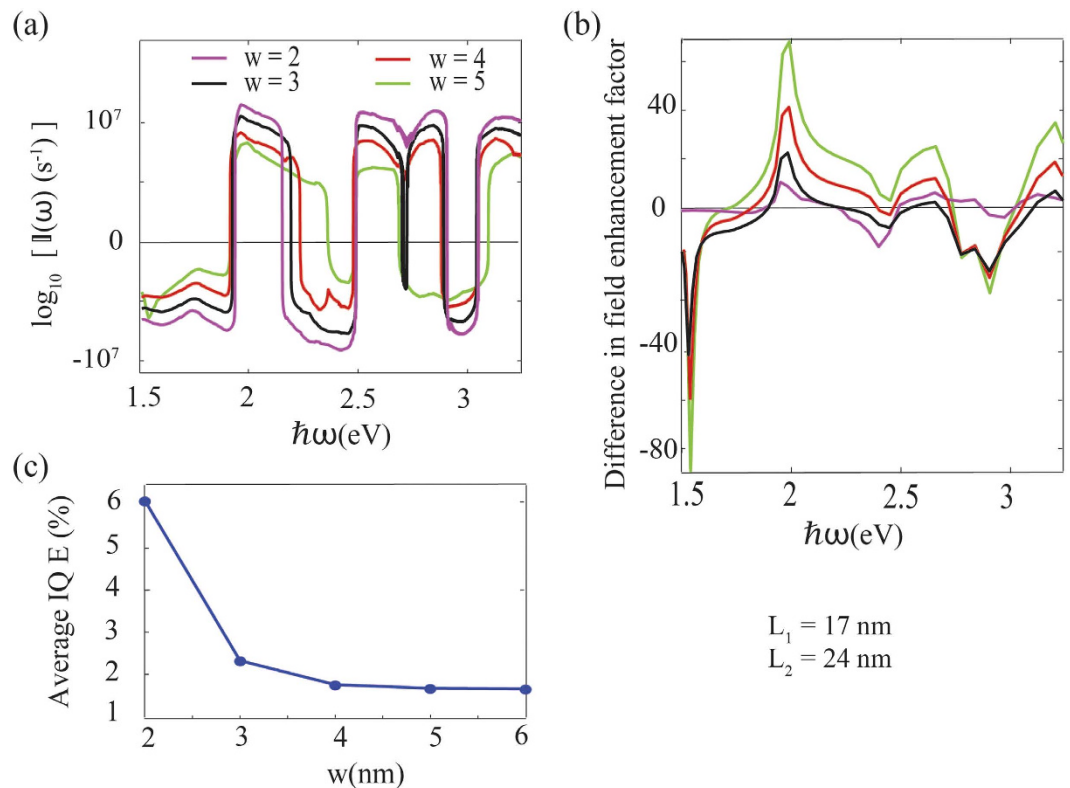
Figure 5. Same as in Fig. 2 except that the barrier width is varied while keeping other parameters constant. (**a**) $\mathbb{I}(\omega)$ for different w. (**b**) Difference in the electric field enhancement factor. (**c**) Averaged quantum efficiency for each case as a function of frequency.

On the other hand, the magnitude of electron flow (averaged over the spectrum) increases with the volume. Therefore, when deciding device dimensions, a compromise between the efficiency and the magnitude of current generated has to be made.

The relative lengths of the nanorods is another important parameter that effects the CDSD performance. A higher geometric difference between the two nanorods (i.e. a larger ζ value) can lead to a higher internal quantum efficiency but it will make the direction of the flow less sensitive to the frequency. Also a larger ζ will result in a higher β value, indicating uneven positive and negative current flows, which can be desirable or undesirable based on the application.

Decreasing the barrier width will exponentially increase the magnitude of the electron flow from the device and its internal quantum efficiency. But if the barrier width is too small, tunnelling breakdown can happen[58], depending on the intensity of the applied electric field, leading to reduced quantum confinement and decreased controllability over the electron flow direction. Further, the difficulty in fabricating very narrow barriers must also be considered. Higher intensity electric fields can lead to an increased $\mathbb{I}(\omega)$ at all incident frequencies. However, the intensity of the electric field is limited in practice by the barrier width. For moderate optical intensities ($\sim 10^7 \, \mathrm{Wm^{-2}}$), a barrier width of about 3 nm is found to be most suitable.

A wide-band-gap semiconductor such as TiO_2, SiC, or ZnO is desirable for constructing the barrier. The upper limit of the operating frequency is limited by the barrier band-gap since electron excitations in the barrier has to be avoided. Also the metal-barrier potential difference should be higher than the metal-external circuit potential in order to control the direction of the flow. For constructing the nanorods, strongly light absorbing plasmonic metals such as silver or gold are most suitable. The lower limit of the operating frequency is decided by the minimum energy that an electron can absorb to surmount the barrier, which is equal to the energy difference between the barrier and the Fermi level of the plasmonic metal.

When designing the proposed CDSD, Eq. (21) can be used to plot $\mathbb{I}(\omega)$ over the entire frequency rage of the incident light for different sets of L_1, L_2, R and w values. Then, based on the trends we have identified in this paper, the parameters, ζ, overall volume of the nanorods and the potential-barrier width can be varied to tune this CDSD to work for certain operating frequencies delivering required amounts of negative and positive currents to the external circuit with a desired quantum efficiency. For the dimensions we have considered in this paper, the proposed CDSD shows an average internal quantum efficiency of over 2%, with peak efficiencies approaching 30% at certain frequencies of incident light. The possibility of increasing the internal quantum efficiency by using more conductive barrier materials needs to be investigated further. Also, other combinations of particle geometries may perform better and improve the performance of such devices.

In our study the injection rate of hot electrons over the barrier is calculated assuming a smooth interface between the metal and the semiconductor. This assumption imposes the condition that the component of

electron's momentum normal to the interface should be large enough for the electron to cross the Schottky barrier. In practice, imperfections and roughness of this interface can change the direction of momentum of incident electrons and enhance the injection rate. Tunneling through the barrier is found to be negligible for the barrier thicknesses we have considered.

Coupled plasmon resonances created by plasmonic nano antennas placed in close proximity to the CDSD can generate internal fields that are enhanced by orders of magnitude, improving the efficiency of the device. The energy from these antennas can be transferred efficiently to the plasmonic nanoparticles non-radiatively through resonance energy transfer[59,60] or radiatively, depending on the distance between the antenna and the CDSD. Cascaded plasmon resonances[61,62], constructed using chains of such geometrically asymmetric antennas having the same plasmon resonance frequency but significantly different volumes, have proven to provide extremely strong internal field enhancements. When such nanoparticles are coupled with each other, a multiplicative field enhancement can be observed predominantly in the smallest particle of the chain. This mechanism can be used to improve the efficiency of the proposed CDSD.

Another experimentally demonstrated method to profoundly improve the electric field enhancement in metal nanoparticles is near-field coupling with an active substrate such as Si[63] or quantum-dot-embedded dielectrics[64]. The energy emitted by electron relaxations in the active medium can be transferred non-radiatively to the surface plasmons in the plasmonic nanoparticle. The stimulated nature of this energy transfer causes buildup of macro-scopic numbers of coherent surface plasmons in the nanoparticle, increasing its internal electric field. This concept can be used to improve the electric field inside the plasmonic nanoparticles in the proposed CDSD, which then acts similar to the resonant cavity in a spaser[65,66].

Methods

Electron excitation probability in nano-particles under an external pertubation.
Prior to the optical excitation, the system is considered to be under a time independent but spatially varying potential $V(\mathbf{r})$. The Schrödinger equation for the motion of an electron in this system has its usual form

$$j\hbar\frac{\partial\Psi(\mathbf{r}, t)}{\partial t} = \widehat{H}\Psi(\mathbf{r}, t), \quad \widehat{H} = -\frac{\hbar^2}{2\mu}\nabla^2 + V(\mathbf{r}), \tag{23}$$

where $\Psi(\mathbf{r}, t)$ is electron's wave function at time t located at a position $\mathbf{r}$, $\widehat{H}$ is the Hamiltonian, and μ is the effective mass of the electron. Since $V(r)$ is time independent, $\Psi(\mathbf{r}, t)$ can be separated into temporal and spatial components as $\Psi(\mathbf{r}, t) = \exp(-j\mathcal{E}t/\hbar)\psi(\mathbf{r})$. By substituting this in Eq. (23), the time independent part of the wave function satisfies the eigenvalue equation

$$\widehat{H}\psi_k(\mathbf{r}) = \mathcal{E}_k\psi_k(\mathbf{r}), \tag{24}$$

where $\mathcal{E}_k$ and $\psi_k(\mathbf{r})$ are the eigenvalues and eigenfunctions of the kth solution of this equation, representing possible electron states.

When light is incident on an electron, its motion of an electron is governed by

$$j\hbar\frac{\partial\Psi'(\mathbf{r}, t)}{\partial t} = \widehat{H}'\Psi'(\mathbf{r}, t), \quad \widehat{H}' = -\frac{\hbar^2}{2\mu}\nabla^2 + V(\mathbf{r}) + V'(t), \tag{25}$$

where $V'(t)$ is the time-dependant perturbing potential causing electronic transitions between its energy states and $\Psi'(\mathbf{r}, t)$ is the modified electron wave function at this stage. We can express $\Psi'(\mathbf{r}, t)$ as an expansion of the eigen functions $\Psi_i(\mathbf{r}, t)$ of the unperturbed, time independent system using a time dependent coefficient $c_i(t)$ as,

$$\Psi'(\mathbf{r}, t) = \sum_i c_i(t)\Psi_i(\mathbf{r}, t) = \sum_i c_i(t)\exp\left(\frac{-j\mathcal{E}_i t}{\hbar}\right)\psi_i(\mathbf{r}). \tag{26}$$

Substituting this equation in Eq. (25), multiplying the resulting expression by $\exp(-j\mathcal{E}_f t/\hbar)\psi_f(\mathbf{r})$, and integrating over the spatial coordinates yields,

$$\frac{\partial c_f(t)}{\partial t} = \frac{1}{j\hbar}\sum_i c_i(t)\exp\left(\frac{jt(\mathcal{E}_f - \mathcal{E}_i)}{\hbar}\right)\langle\psi_f(\mathbf{r})|V'(\mathbf{r}, t)|\psi_i(\mathbf{r})\rangle. \tag{27}$$

The quantity $|c_f(t)|^2$ represents the time-dependent transition probability of an electron from an initial energy state i a final state f. It is given by[33,34],

$$P_{if}(t) = \left|-\frac{j}{\hbar}\int_0^t \langle\psi_f(\mathbf{r})|V'(\mathbf{r}, t')|\psi_i(\mathbf{r})\rangle \exp(i\omega_{fi}t')\mathrm{d}t'\right|^2. \tag{28}$$

with ω_{fi} representing the energy difference between the final and initial states.

Derivation of energy eigenstates of an electron inside a nanorod.
By solving Eq. (11) for the radial and azimuthal potentials given in Eq. (12), the quantized electron energy in these directions can be easily found as[67]

$$\mathcal{E}_{n,m} = \hbar^2\pi^2/(8\mu)[(2n + |m| + 3/2)^2/R^2].$$

(29)

The longitudinal part of energy containing the quantum number l is more complicated owing to the finite nature of longitudinal boundaries.

To find the longitudinal wave functions $\psi_{li}(z)$ and $\psi_{lf}(z)$ and the corresponding energy components $\mathcal{E}_{li}$ and $\mathcal{E}_{lf}$, we assume that prior to excitation electrons reside in an energy state below the Fermi level $\mathcal{E}_F$, which is less than both U_1 and U_2, and all final energy states have energies larger than U_1 and U_2. Two sets of solutions needs to be found for Eq. (11) for these two situations[33]

Consider first the initial state. Since $\mathcal{E}_{li}$ is less than U_1 and U_2, the wave function $\psi_{li}(z)$ can be written in the form

$$\psi_{li}(z) = \begin{cases} A_{li} \exp(k_{1li}z), & z < 0 \\ C_{li} \exp(jk_{2li}z) + D_{li} \exp(-jk_{2li}z), & 0 \geq z \geq L, \\ E_{li} \exp(-k_{3li}z), & z > L \end{cases}$$

(30)

where

$$k_{1li} = \sqrt{2\mu(U_1 - \mathcal{E}_{li})/\hbar^2}, \quad k_{2li} = \sqrt{2\mu\mathcal{E}_{li}/\hbar^2}, \quad k_{3li} = \sqrt{2\mu(U_2 - \mathcal{E}_{li})/\hbar^2}.$$

(31)

The constants C_{li}, D_{li} and E_{li} can be found in terms of A_{li} considering the continuity of the wave function and its first derivative at the boundaries and are given by

$$C_{li} = (k_{2li} - jk_{1li})\frac{A}{2k_{2li}},$$

$$D_{li} = (k_{2li} + jk_{1li})\frac{A}{2k_{2li}},$$

$$E_{li} = [k_{2li} \cos(k_{2li}a) + k_{1li} \sin(k_{2li}a)]\frac{Ae^{-k_{3li}a}}{2k_{2li}}.$$

(32)

The value of A_{li} is found using the normalization $\int_{-\infty}^{\infty} |\psi_{li}(z)|^2 dz = 1$ to be

$$A_{li} = \left[\frac{1}{2k_{1li}} + \sin^2(k_{2li}L)\frac{k_{1li}}{k_{2li}^2} - [\sin(2k_{2li}L) - 2k_{2li}L]\frac{k_{1li}^2}{4k_{2li}^3} \right.$$

$$+ [\sin(2k_{2li}L) + 2k_{2li}L]\frac{1}{4k_{2li}}$$

$$\left. + \left(\cos(k_{2li}L) + \frac{k_{1li}}{k_{2li}} \sin(k_{2li}L)\right)^2\left(\frac{1}{2k_{3li}}\right) \right]^{-\frac{1}{2}}.$$

(33)

The quantized energy levels ε_{li} are found numerically from the eigenvalue equation

$$\tan\left(\sqrt{\frac{2\mu}{\hbar^2}\mathcal{E}_{li}}L\right) - \frac{(\sqrt{U_2 - \mathcal{E}_{li}} + \sqrt{U_1 - \mathcal{E}_{li}})\sqrt{\mathcal{E}_{li}}}{\mathcal{E}_{li} - \sqrt{U_1 - \mathcal{E}_{li}}\sqrt{U_2 - \mathcal{E}_{li}}} = 0.$$

(34)

When $\mathcal{E}_{li} < U_1$ and $\mathcal{E}_{li} < U_2$, total energy of an electron in the state i can be written as

$$\mathcal{E}_i = \frac{\hbar^2\pi^2}{8\mu}\left[\frac{(2ni + |mi| + 3/2)^2}{R^2}\right] + \mathcal{E}_{li}.$$

(35)

Consider now the final state. Since $\mathcal{E}_{lf}$ is greater than U_1 and U_2, $\psi_{lf}(\mathbf{r})$ is of the form

$$\psi_{lf}(z) = \begin{cases} A_{lf} \exp(jk_{1lf}z), & z < 0 \\ C_{lf} \exp(jk_{2lf}z) + D \exp(-jk_{2lf}z), & z \geq 0, \\ E_{lf} \exp(-jk_{3lf}z), & z > L \end{cases}$$

(36)

where

$$k_{1lf} = \sqrt{2\mu(\mathcal{E}_{lf} - U_1)/\hbar^2}, \quad k_{2lf} = \sqrt{2\mu\mathcal{E}_{lf}/\hbar^2}, \quad k_{3lf} = \sqrt{2\mu(\mathcal{E}_{lf} - U_2)/\hbar^2}.$$

(37)

As before, the constants C_{lf}, D_{lf} and E_{lf} can be found in terms of A_{lf} considering the continuity of the wave function and its derivative at the boundaries:

$$C_{lf} = (k_{1lf} + k_{2lf})\frac{A_{lf}}{2k_{2lf}}, \quad D_{lf} = (k_{2lf} - k_{1lf})\frac{A_{lf}}{2k_{2lf}}, \quad E = k_{2lf}A_{lf}/e^{-j(k_{2lf} - k_{3lf})L}. \tag{38}$$

However, since there is no bounding potential, A_{lf} is not normalizable. Therefore, to find A_{lf} we introduce a fictitious length of confinement L_{inf} which is removed at a later stage. After applying the orthonormal conditions within this length, A_{lf} is found to be $A_{lf} = \Lambda L_{\text{inf}}^{-\frac{1}{2}}$ where

$$\Lambda = \left[1 + \left(\cos(k_{2lf}L)\cos(k_{3lf}L) + \frac{k_{1lf}}{k_{2lf}} \sin(k_{2lf}L)\sin(k_{3lf}L) \right)^2 \right. $$
$$\left. + \left(-\cos(k_{2lf}L)\sin(k_{3lf}L) + \frac{k_{1lf}}{k_{2lf}} \sin(k_{2lf}L)\cos(k_{3lf}L) \right)^2 \right]^{-\frac{1}{2}}. \tag{39}$$

We define two new quantities,

$$\overline{C_{lf}} = C_{lf}\sqrt{L_{\text{inf}}} = (k_{1lf} + k_{2lf})\Lambda/(2k_{2lf}), \quad \bar{D}_{lf} = D_{lf}\sqrt{L_{\text{inf}}} = (k_{2lf} - k_{1lf})\Lambda/(2k_{2lf}), \tag{40}$$

which are independent of the fictitious length of confinement L_{inf} and are used later. Finally, the total energy $\mathcal{E}_f$ can be written as

$$\mathcal{E}_f = \frac{\hbar^2\pi^2}{8\mu}\left[\frac{(2nf + |mf| + 3/2)^2}{R^2} \right] + \mathcal{E}_{lf}. \tag{41}$$

Note that $\mathcal{E}_f$ is not quantized in the z direction because $\mathcal{E}_{lf}$ is continuous with values greater than both U_1 and U_2.

Internal quantum efficiency. Internal Quantum efficiency of a CDSD can be defined as the ratio of the rate of electron injection to the external circuit $(\mathbb{I}(\omega))$ and the rate of photon absorption $(\mathbb{I}(\omega)_{\text{ph}})$ given by

$$\mathbb{I}(\omega)_{\text{ph}} = \frac{\mathbb{P}(\omega)_{\text{absorbed}}}{\hbar\omega} = \frac{\omega V \; \text{Im}(\varepsilon(\omega))(\gamma(\omega)E_0)^2}{2\hbar\omega}, \tag{42}$$

where V is the volume of the particle, $\text{Im}(\varepsilon(\omega))$ is the imaginary part of the dielectric permittivity and $\mathbb{P}(\omega)_{\text{absorbed}}$ is the power absorbed.

Material parameters. In all calculations we assume the nano-particles to be made of silver with a Fermi energy of 5.5 eV. The semiconductor is taken to be TiO$_2$, creating a barrier of 0.8 eV. The mobility of electrons in TiO$_2$ is taken as $1\, cm^2\, V^{-1}\, s^{-1}$ [68,69]. The complex permittivity of silver is taken from experimental data [70] and the surrounding medium is assumed to be air with a relative permittivity of 1. The illumination intensity is taken as $3.6 \times 10^7\, \text{Wm}^{-2}$.

References

1. Govorov, A. O., Zhang, H., Demir, H. V. & Gun'ko, Y. K. Photogeneration of hot plasmonic electrons with metal nanocrystals: Quantum description and potential applications. *Nano Today* **9,** 85–101 (2014).
2. Kumarasinghe, C. S., Premaratne, M., Bao, Q. & Agrawal, G. P. Theoretical analysis of hot electron dynamics in nanorods. *Scientific reports* **5,** 12140 (2015).
3. Mubeen, S. *et al.* An autonomous photosynthetic device in which all charge carriers derive from surface plasmons. *Nature nanotechnology* **8,** 247–251 (2013).
4. Zhang, N., Liu, S., Fu, X. & Xu, Y.-J. Synthesis of m@ tio2 (m = au, pd, pt) core-shell nanocomposites with tunable photoreactivity. *The Journal of Physical Chemistry C* **115,** 9136–9145 (2011).
5. Lee, Y. K. *et al.* Surface plasmon-driven hot electron flow probed with metal-semiconductor nanodiodes. *Nano letters* **11,** 4251–4255 (2011).
6. Conklin, D. *et al.* Exploiting plasmon-induced hot electrons in molecular electronic devices. *ACS nano* **7,** 4479–4486 (2013).
7. Lee, J., Mubeen, S., Ji, X., Stucky, G. D. & Moskovits, M. Plasmonic photoanodes for solar water splitting with visible light. *Nano letters* **12,** 5014–5019 (2012).
8. Gomes Silva, C., Juárez, R., Marino, T., Molinari, R. & Garcia, H. Influence of excitation wavelength (uv or visible light) on the photocatalytic activity of titania containing gold nanoparticles for the generation of hydrogen or oxygen from water. *Journal of the American Chemical Society* **133,** 595–602 (2010).
9. Giugni, A. *et al.* Hot-electron nanoscopy using adiabatic compression of surface plasmons. *Nature nanotechnology* **8,** 845–852 (2013).
10. Landy, N., Sajuyigbe, S., Mock, J., Smith, D. & Padilla, W. Perfect metamaterial absorber. *Physical review letters* **100,** 207402 (2008).
11. Kumarasinghe, C., Premaratne, M. & Agrawal, G. P. Dielectric function of spherical dome shells with quantum size effects. *Optics express* **22,** 11966–11984 (2014).
12. Hattori, H. T. *et al.* In-plane coupling of light from inp-based photonic crystal band-edge lasers into single-mode waveguides. *Quantum Electronics, IEEE Journal of* **43,** 279–286 (2007).
13. El-Sayed, M. A. Small is different: shape-, size-, and composition-dependent properties of some colloidal semiconductor nanocrystals. *Accounts of chemical research* **37,** 326–333 (2004).

14. Rammelt, U., Hebestreit, N., Fikus, A. & Plieth, W. Investigation of polybithiophene/n-tio 2 bilayers by electrochemical impedance spectroscopy and photoelectrochemistry. *Electrochimica acta* **46,** 2363–2371 (2001).
15. Beranek, R. & Kisch, H. A hybrid semiconductor electrode for wavelength-controlled switching of the photocurrent direction. *Angewandte Chemie International Edition* **47,** 1320–1322 (2008).
16. Chen, H., Liu, G. & Wang, L. Switched photocurrent direction in au/tio2 bilayer thin films. *Scientific reports* **5** (2015).
17. Yasutomi, S., Morita, T., Imanishi, Y. & Kimura, S. A molecular photodiode system that can switch photocurrent direction. *Science* **304,** 1944–1947 (2004).
18. Matsui, J., Mitsuishi, M., Aoki, A. & Miyashita, T. Molecular optical gating devices based on polymer nanosheets assemblies. *Journal of the American Chemical Society* **126,** 3708–3709 (2004).
19. Nitahara, S., Akiyama, T., Inoue, S. & Yamada, S. A photoelectronic switching device using a mixed self-assembled monolayer. *The Journal of Physical Chemistry B* **109,** 3944–3948 (2005).
20. Matsui, J., Abe, K., Mitsuishi, M., Aoki, A. & Miyashita, T. Quasi-solid-state optical logic devices based on redox polymer nanosheet assembly. *Langmuir* **25,** 11061–11066 (2009).
21. Zheng, Z. *et al.* Facile *in situ* synthesis of visible-light plasmonic photocatalysts m@ tio 2 (m = au, pt, ag) and evaluation of their photocatalytic oxidation of benzene to phenol. *Journal of Materials Chemistry* **21,** 9079–9087 (2011).
22. Yokomizo, Y., Krishnamurthy, S. & Kamat, P. V. Photoinduced electron charge and discharge of graphene-zno nanoparticle assembly. *Catalysis Today* **199,** 36–41 (2013).
23. Hartland, G. V. Measurements of the material properties of metal nanoparticles by time-resolved spectroscopy. *Physical Chemistry Chemical Physics* **6,** 5263–5274 (2004).
24. Voisin, C., Del Fatti, N., Christofilos, D. & Vallee, F. Ultrafast electron dynamics and optical nonlinearities in metal nanoparticles. *The Journal of Physical Chemistry B* **105,** 2264–2280 (2001).
25. Inouye, H., Tanaka, K., Tanahashi, I. & Hirao, K. Ultrafast dynamics of nonequilibrium electrons in a gold nanoparticle system. *Physical Review B* **57,** 11334 (1998).
26. Kang, Y. *et al.* Plasmonic hot electron induced structural phase transition in a mos2 monolayer. *Advanced Materials* **26,** 6467–6471 (2014).
27. Fowler, R. H. The analysis of photoelectric sensitivity curves for clean metals at various temperatures. *Physical Review* **38,** 45 (1931).
28. Knight, M. W. *et al.* Embedding plasmonic nanostructure diodes enhances hot electron emission. *Nano letters* **13,** 1687–1692 (2013).
29. Frese, K. W. & Chen, C. Theoretical models of hot carrier effects at metal-semiconductor electrodes. *Journal of The Electrochemical Society* **139,** 3234–3243 (1992).
30. Dowgiallo, A.-M., Schwartzberg, A. M. & Knappenberger Jr., K. L. Structure-dependent coherent acoustic vibrations of hollow gold nanospheres. *Nano letters* **11,** 3258–3262 (2011).
31. Govorov, A. O., Zhang, H. & Gun'ko, Y. K. Theory of photoinjection of hot plasmonic carriers from metal nanostructures into semiconductors and surface molecules. *The Journal of Physical Chemistry C* **117,** 16616–16631 (2013).
32. Manjavacas, A., Liu, J. G., Kulkarni, V. & Nordlander, P. Plasmon-induced hot carriers in metallic nanoparticles. *ACS nano* **8,** 7630–7638 (2014).
33. Zettili, N. *Quantum mechanics: concepts and applications* (John Wiley & Sons, 2009).
34. Kaviany, M. *Heat transfer physics* (Cambridge University Press, 2014).
35. Reggiani, L. *et al. Hot-electron transport in semiconductors*, vol. 58 (Springer Science & Business Media, 2006).
36. Sapoval, B., Hermann, C. & Hermann, C. *Physics of semiconductors* (Springer Science & Business Media, 2003).
37. Ozawa, K. *et al.* Electron-hole recombination time at tio2 single-crystal surfaces: Influence of surface band bending. *The Journal of Physical Chemistry Letters* **5,** 1953–1957 (2014).
38. Albery, W. J. & Bartlett, P. N. The transport and kinetics of photogenerated carriers in colloidal semiconductor electrode particles. *Journal of the Electrochemical Society* **131,** 315–325 (1984).
39. Ungureanu, C., Rayavarapu, R. G., Manohar, S. & van Leeuwen, T. G. Discrete dipole approximation simulations of gold nanorod optical properties: Choice of input parameters and comparison with experiment. *Journal of Applied Physics* **105,** 102032 (2009).
40. Attanayake, T., Premaratne, M. & Agrawal, G. P. Characterizing the optical response of symmetric hemispherical nano-dimers. *Plasmonics* 1–14 (2015).
41. Venermo, J. & Sihvola, A. Dielectric polarizability of circular cylinder. *Journal of electrostatics* **63,** 101–117 (2005).
42. DePrince, A. E. & Hinde, R. J. Accurate computation of electric field enhancement factors for metallic nanoparticles using the discrete dipole approximation. *Nanoscale research letters* **5,** 592–596 (2010).
43. Grynberg, G., Aspect, A. & Fabre, C. *Introduction to quantum optics: from the semi-classical approach to quantized light* (Cambridge university press, 2010).
44. Dweydari, A. & Mee, C. Work function measurements on (100) and (110) surfaces of silver. *physica status solidi (a)* **27,** 223–230 (1975).
45. Könenkamp, R. & Rieck, I. Electrical properties of schottky diodes on nano-porous tio 2 films. *Materials Science and Engineering: B* **69,** 519–521 (2000).
46. Aydinoglu, F. *et al.* Higher performance metal-insulator-metal diodes using multiple insulator layers. *Austin J. Nanomed. Nanotechnol.* **1** (2013).
47. Könenkamp, R. Carrier transport in nanoporous tio 2 films. *Physical Review B* **61,** 11057 (2000).
48. Zhao, J. H., Sheng, K. & Lebron-Velilla, R. C. Silicon carbide schottky barrier diode. *International journal of high speed electronics and systems* **15,** 821–866 (2005).
49. Davydov, S. Y. On the electron affinity of silicon carbide polytypes. *Semiconductors* **41,** 696–698 (2007).
50. Esteban, R., Borisov, A. G., Nordlander, P. & Aizpurua, J. Bridging quantum and classical plasmonics with a quantum-corrected model. *Nature communications* **3,** 825 (2012).
51. Groeneveld, R. H., Sprik, R. & Lagendijk, A. Femtosecond spectroscopy of electron-electron and electron-phonon energy relaxation in ag and au. *Physical Review B* **51,** 11433 (1995).
52. Voisin, C. *et al.* Size-dependent electron-electron interactions in metal nanoparticles. *Physical review letters* **85,** 2200 (2000).
53. Anisimov, S., Kapeliovich, B. & Perelman, T. Electron emission from metal surfaces exposed to ultrashort laser pulses. *Zh. Eksp. Teor. Fiz* **66,** 375–377 (1974).
54. Anisimov, S. Effect of powerful light (laser) fluxes on metals. *Zhur. Tekhn. Fiziki* **36,** 1273–83 (1966).
55. Mahmoud, M. A., O'Neil, D. & El-Sayed, M. A. Shape-and symmetry-dependent mechanical properties of metallic gold and silver on the nanoscale. *Nano letters* **14,** 743–748 (2014).
56. Aizpurua, J. *et al.* Optical properties of coupled metallic nanorods for field-enhanced spectroscopy. *Physical Review B* **71,** 235420 (2005).
57. Lee, F., Lee, K., Lai, S., Cheng, Y. & Hsu, T. Electric field enhancement near surface irregularities. *Solid state communications* **63,** 299–302 (1987).
58. Wu, K., Rodrguez-Córdoba, W. E., Yang, Y. & Lian, T. Plasmon-induced hot electron transfer from the au tip to cds rod in cds-au nanoheterostructures. *Nano letters* **13,** 5255–5263 (2013).
59. Weeraddana, D., Premaratne, M. & Andrews, D. L. Direct and third-body mediated resonance energy transfer in dimensionally constrained nanostructures. *Physical Review B* **92,** 035128 (2015).
60. Li, J. *et al.* Plasmon-induced resonance energy transfer for solar energy conversion. *Nature Photonics* **9,** 601–607 (2015).

61. Li, K., Stockman, M. I. & Bergman, D. J. Self-similar chain of metal nanospheres as an efficient nanolens. *Physical review letters* **91,** 227402 (2003).
62. Toroghi, S. & Kik, P. G. Cascaded field enhancement in plasmon resonant dimer nanoantennas compatible with two-dimensional nanofabrication methods. *Applied Physics Letters* **101,** 013116 (2012).
63. Guo, S.-H. *et al.* The effect of an active substrate on nanoparticle-enhanced fluorescence. *Advanced Mmaterials-Deerfield Beach Then Weinheim-* **20,** 1424 (2008).
64. Zheludev, N. I., Prosvirnin, S., Papasimakis, N. & Fedotov, V. Lasing spaser. *Nature Photonics* **2,** 351–354 (2008).
65. Bergman, D. J. & Stockman, M. I. Surface plasmon amplification by stimulated emission of radiation: quantum generation of coherent surface plasmons in nanosystems. *Physical review letters* **90,** 027402 (2003).
66. Jayasekara, C., Premaratne, M., Stockman, M. I & Gunapala, S. D. Multimode analysis of highly tunable, quantum cascade powered, circular graphene spaser. *Journal of Applied Physics* **118,** 173101 (2015).
67. Nunes, O., Agrello, D. & Fonseca, A. Thermoelectric amplification of phonons in cylindrical quantum well wires. *Journal of applied physics* **83,** 87–89 (1998).
68. Hendry, E., Koeberg, M., Pijpers, J. & Bonn, M. Reduction of carrier mobility in semiconductors caused by charge-charge interactions. *Physical Review B* **75,** 233202 (2007).
69. Hendry, E., Koeberg, M., O'Regan, B. & Bonn, M. Local field effects on electron transport in nanostructured tio2 revealed by terahertz spectroscopy. *Nano letters* **6,** 755–759 (2006).
70. Johnson, P. B. & Christy, R.-W. Optical constants of the noble metals. *Physical Review B* **6,** 4370 (1972).

Acknowledgements

Author Contributions

C.S.K. performed analytical calculations and analyzed the obtained expressions, drew the figures, and prepared the first draft of the manuscript. M.P., S.D.G. and G.P.A. supervised the study, contributed to the analysis and interpretation of the results, helped to formulate and present the research outcomes, and thoroughly edited the manuscript.

Additional Information

Competing financial interests: The authors declare no competing financial interests.

How to cite this article: Kumarasinghe, C. S. *et al.* Design of all-optical, hot-electron current-direction-switching device based on geometrical asymmetry. *Sci. Rep.* **6,** 21470; doi: 10.1038/srep21470 (2016).